The Astrophysical Journal Letters, 957:L28 (6pp), 2023 November 10 https://doi.org/10.3847/2041-8213/ad0730

AC Her: Evidence of the First Polar Circumbinary Planet

Rebecca G. Martin[1,2], Stephen H. Lubow[3], David Vallet[1,2], Narsireddy Anugu[4], and Douglas R. Gies[5]
[1] Nevada Center for Astrophysics, University of Nevada, Las Vegas, 4505 South Maryland Parkway, Las Vegas, NV 89154, USA
[2] Department of Physics and Astronomy, University of Nevada, Las Vegas, 4505 South Maryland Parkway, Las Vegas, NV 89154, USA
[3] Space Telescope Science Institute, 3700 San Martin Drive, Baltimore, MD 21218, USA
[4] The CHARA Array of Georgia State University, Mount Wilson Observatory, Mount Wilson, CA 91023, USA
[5] Center for High Angular Resolution Astronomy and Department of Physics and Astronomy, Georgia State University, P.O. Box 5060, Atlanta, GA 30302-5060, USA
Received 2023 September 7; revised 2023 October 9; accepted 2023 October 25; published 2023 November 8

Abstract

We examine the geometry of the post–asymptotic giant branch (AGB) star binary AC Her and its circumbinary disk. We show that the observations describe a binary orbit that is perpendicular to the disk with an angular momentum vector that is within 9° of the binary eccentricity vector, meaning that the disk is close to a stable polar alignment. The most likely explanation for the very large inner radius of the dust is a planet within the circumbinary disk. This is therefore both the first reported detection of a polar circumbinary disk around a post-AGB binary and the first evidence of a polar circumbinary planet. We consider the dynamical constraints on the circumbinary disk size and mass. The polar circumbinary disk feeds circumstellar disks with gas on orbits that are highly inclined with respect to the binary orbit plane. The resulting circumstellar disk inclination could be anywhere from coplanar to polar depending upon the competition between the mass accretion and binary torques.

Unified Astronomy Thesaurus concepts: Accretion (14); Binary stars (154); Hydrodynamics (1963); Exoplanet formation (492); Post-asymptotic giant branch stars (2121)

1. Introduction

Many post–asymptotic giant branch (AGB) stars have a disk that is Keplerian and stable (de Ruyter et al. 2006; Bujarrabal et al. 2013; Gallardo Cava et al. 2021). All post-AGB stars with a disk are in a binary and the disk is circumbinary (Bujarrabal et al. 2013; Izzard & Jermyn 2018). The disk may be formed in the wind of the parent star, during nonconservative mass transfer or common envelope ejection (e.g., Kashi & Soker 2011; Izzard & Jermyn 2023). The binaries have orbital periods in the range 100–3000 days (Oomen et al. 2018) and eccentricities up to about 0.6, which may be a natural outcome of the stellar evolution process and binary–disk interactions (Sepinsky et al. 2007a, 2007b; Dermine et al. 2013; Oomen et al. 2020; D'Orazio & Duffell 2021; Zrake et al. 2021). The disks are remarkably similar to protoplanetary disks with masses up to about $0.01\,M_\odot$ and sizes up to about 1000 au (Sahai et al. 2011; Bujarrabal et al. 2015). The accretion rate from the inner edge of the circumbinary disk is up to about $10^{-7}\,M_\odot\,\mathrm{yr}^{-1}$ (Bujarrabal et al. 2018; Bollen et al. 2020).

Around 10% of the post-AGB circumbinary disks have a lack of near-infrared excess (Kluska et al. 2022; Corporaal et al. 2023), similar to transition disks around main-sequence stars. AC Her (Van Winckel et al. 1998; Gielen et al. 2007) is an example of a post-AGB binary system with a large inner hole in the dust. The observed binary and disk parameters of the system are shown in Table 1 that is based on values given in Hillen et al. (2015) and Anugu et al. (2023). The inner edge of the dust disk is about 10 times the binary separation (Hillen et al. 2015), much farther out than the radius where tidal truncation from the binary would predict the inner disk edge (e.g., Artymowicz & Lubow 1994; Hirsh et al. 2020) and much farther out than the expected dust sublimation radius (Kluska et al. 2019). The best explanation for the large hole in the dust is the presence of a circumbinary planet (e.g., Kluska et al. 2022; Anugu et al. 2023) that creates a pressure maximum in the disk and traps dust grains while allowing gas to flow past the planet (e.g., Pinilla et al. 2012, 2016; Zhu et al. 2013; Francis & van der Marel 2020).

In Section 2 we examine the geometry of the AC Her system and show that the circumbinary disk is highly misaligned to the binary orbit. In fact, the disk is close to alignment with the binary eccentricity vector, a configuration known as polar alignment (see the left panel of Figure 1). This is a stable state for a circumbinary disk around an eccentric binary (Aly et al. 2015; Martin & Lubow 2017; Lubow & Martin 2018; Zanazzi & Lai 2018; Cuello & Giuppone 2019; Smallwood et al. 2020; Rabago et al. 2023). Previously, there have been observations of two polar aligned circumbinary gas disks (Kennedy et al. 2019; Kenworthy et al. 2022) and one debris disk (Kennedy et al. 2012) around eccentric main-sequence star binaries. The existence of these polar circumbinary disks suggests that planet formation in a polar configuration may be possible. However, to date, all the observed circumbinary planets are close to coplanar to the binary orbital plane (e.g., Doyle et al. 2011; Orosz et al. 2012; Welsh et al. 2012). This is likely a result of selection effects (Martin & Triaud 2015; Martin 2017; Czekala et al. 2019). In Section 3, we discuss the evidence for the first polar circumbinary planet. In Section 4 we discuss the implications for a polar aligned disk in the AC Her system. We draw our conclusions in Section 5.

2. Orientation of the Disk Relative to the Binary Orbit

In this section we determine the orientation of the circumbinary disk relative to the orbit of the eccentric binary. The observed binary inclination relative to the plane of the sky,

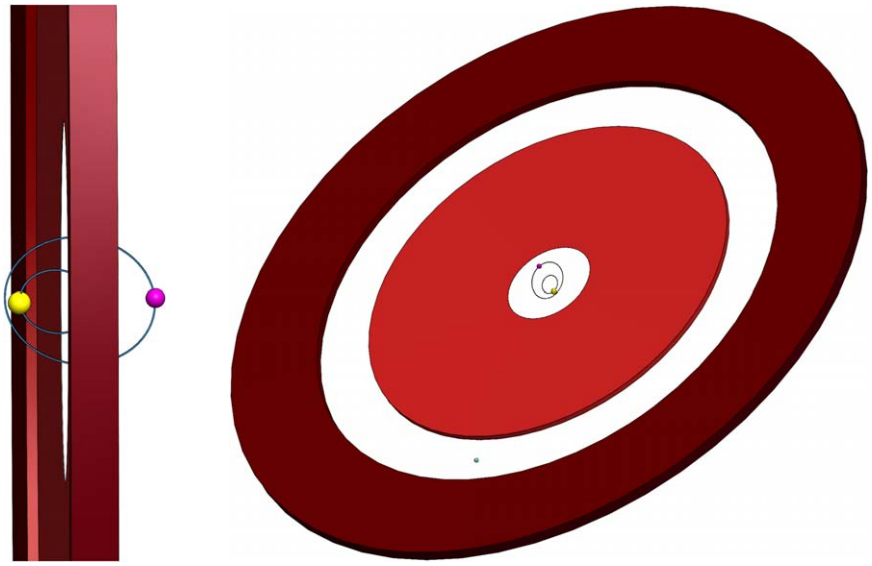

Figure 1. 3D visualizations showing two different views of the AC Her binary system with a polar circumbinary disk. The disk has two parts that are separated by the gap that the putative planet has cleared out. The orbital radius of the planet is shown at 8 a_b (Section 3). The outer disk (dark red) is the gas and dust disk that is observed (Section 2). The outer edge of the observed disk extends beyond what is shown in the figure. The possible inner disk (light red) is a dust depleted disk that has not been observed (Section 3). The inner disk is shown to extend from 1.6 a_b to 7 a_b. The post-AGB star (magenta sphere) and the companion (yellow sphere) are shown at apastron separation. The binary orbits are to scale relative to each other but the sizes of the stars and the planet are not. The left panel shows a view with the disk almost edge on and right panel shows the observed view in the plane of the sky. AC Her is located at a distance of 1402 pc (Gaia Collaboration et al. 2016). The observationally inferred binary semimajor axis is $a_b = 2.01$ mas $= 2.83$ au (Anugu et al. 2023).

Table 1
Parameters of the AC Her Binary Star System

Parameters of the AC Her System	Symbol	Value	Uncertainty
Binary star parameters from Anugu et al. (2023)			
Mass of post-AGB star	M_1	0.73 $M_\odot$	$\pm$0.13 $M_\odot$
Mass of companion star	M_2	1.4 $M_\odot$	$\pm$0.12 $M_\odot$
Binary semimajor axis	a_b	2.83 au	$\pm$0.08 au
Binary eccentricity	e_b	0.206	$\pm$0.004
Binary inclination	i_b	142.°9	$\pm$1.°1
Binary longitude of ascending node	Ω_b	155.°1	$\pm$1.°8
Binary argument of periastron	ω_b	118.°6	$\pm$2°
Disk parameters from Hillen et al. (2015)			
Disk inclination	i_d	50°	$\pm$8°
Disk longitude of ascending node	Ω_d	125°	$\pm$10°
Quantities calculated in this work			
Inclination of disk relative to binary	i_{bd}	96.°5	⋯
Longitude of ascending node of disk relative to binary	Ω_{bd}	84.°1	⋯
Inclination of the disk relative to the binary eccentricity vector	i_{polar}	8.°7	⋯

i_b, longitude of ascending node relative to north, Ω_b, and argument of periastron, ω_b, are given in Table 1. The observed disk inclination, i_d, and longitude of ascending node, Ω_d, are also given for the disk in Table 1. The value of Ω_d is determined by the position angle of the disk as we describe later. The position angle has been determined in two independent ways. Hillen et al. (2015) determined a position angle 125° by using MID-infrared Interferometric instrument (MIDI) on the Very Large Telescope Interferometer (see their Figure 7). Gallardo Cava et al. (2021) determined a position angle of 136.°1 on larger scales based on CO emission line velocity information (see their Figure C.2). The disk argument of periastron is not given because it is assumed to be circular.

We consider a Cartesian coordinate system (x, y, z) in which the x-axis is along the north direction ($\Omega = 0$) in the plane of the sky and the z-axis is along the line of sight toward the observer. The unit binary and disk angular momentum vectors are respectively given by

$$\hat{\boldsymbol{l}}_b = (\sin i_b \sin \Omega_b,\ -\sin i_b \cos \Omega_b,\ \cos i_b)$$
$$\hat{\boldsymbol{l}}_d = (\sin i_d \sin \Omega_d,\ -\sin i_d \cos \Omega_d,\ \cos i_d), \quad (1)$$

where $\hat{}$ denotes a unit vector. The unit eccentricity vector of the binary is

$$\hat{\boldsymbol{e}}_b = (u_{bx},\ u_{by},\ u_{bz}) \quad (2)$$

with

$$u_{bx} = \cos \omega_b \cos \Omega_b - \cos i_b \sin \omega_b \sin \Omega_b$$
$$u_{by} = \cos \omega_b \sin \Omega_b + \cos i_b \sin \omega_b \cos \Omega_b$$
$$u_{bz} = \sin i_b \sin \omega_b. \quad (3)$$

Using the binary and disk angular momentum unit vectors given by Equation (1), we calculate the orientation of the disk relative to the binary. The inclination of the disk relative to the binary is

$$i_{bd} = \cos^{-1}(\hat{\boldsymbol{l}}_b \cdot \hat{\boldsymbol{l}}_d), \quad (4)$$

which agrees with Equation (1) of Czekala et al. (2019). The longitude of ascending node of the disk relative to the binary eccentricity vector is

$$\Omega_{bd} = \tan^{-1}\left[\frac{(\hat{\boldsymbol{l}}_b \times \hat{\boldsymbol{e}}_b) \cdot \hat{\boldsymbol{l}}_d}{\hat{\boldsymbol{l}}_b \cdot \hat{\boldsymbol{l}}_d}\right] + \frac{\pi}{2}, \quad (5)$$

where $\hat{e}_b$ is given by Equation (2) (e.g., Chen et al. 2019, 2020). The misalignment of the disk from polar

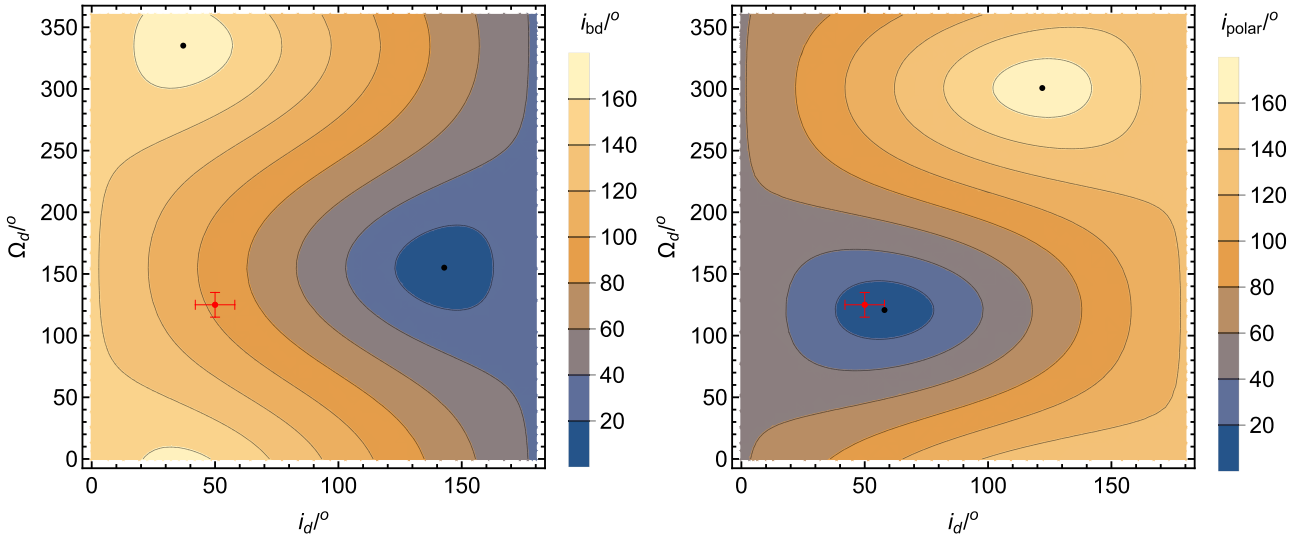

Figure 2. The contours show the inclination of the disk relative to the binary angular momentum vector (i_{bd}, left) and relative to the binary eccentricity vector (i_{polar}, right) as a function of the observed disk inclination i_d and longitude of ascending node Ω_d. The red crosses show the possible disk parameters from Hillen et al. (2015). The black points on the left panel show a coplanar disk ($i_{bd} = 0°$, lower point) and a retrograde coplanar disk ($i_{bd} = 180°$, upper point). The black points on the right panel show a polar aligned disk ($i_{bd} = \Omega_{bd} = 90°$, lower point) and an antipolar aligned disk ($i_{bd} = 90°$ and $\Omega_{bd} = 270°$, upper point).

alignment, or in other words, the inclination of the disk to the binary eccentricity vector, is

$$i_{\rm polar} = \cos^{-1}(\hat{\boldsymbol{l}}_{\rm d} \cdot \hat{\boldsymbol{e}}_{\rm b}). \quad (6)$$

The possible values of $\Omega_{\rm d}$ determined by the imaging of Hillen et al. (2015) are constrained to lie along a line at the position angle. There is then an ambiguity in the value of $\Omega_{\rm d}$ by a shift of 180°. This arises because these observations cannot distinguish an ascending node from a descending node. Hillen et al. (2015) give position angles of 125° and 305° with $i_{\rm d} = 50°$ in both cases. In addition, there is an ambiguity in inclination $i_{\rm d}$ that can take on complementary values. Possible values of ($i_{\rm d}$, $\Omega_{\rm d}$) are (50°, 125°), (130°, 305°), (50°, 305°), and (130°, 125°). By comparing radiative transfer disk models to data, Hillen et al. (2015) conclude that the east side of the disk is farther away (see their Figures 7 and 8). This constraint eliminates the latter two configurations.

The degeneracy in the two possible solutions is broken by using the CO emission line velocity information provided in the studies by Bujarrabal et al. (2015) and Gallardo Cava et al. (2021). While Hillen et al. (2015) studied the disk out a few hundred astronomical units, the velocity studies probed a complementary region that is larger, extending out to about 1000 au. In the velocity studies, the disk inclination was found to be $i_{\rm d} = 45°$ and position angle was determined to be about 135°. The similarity of the position angle to the Hillen et al. (2015) value suggests that the disk orientation does not undergo large changes from the inner to outer regions. Both Figure 2 of Bujarrabal et al. (2015) and Figure 2 of Gallardo Cava et al. (2021) provide the line-of-sight velocity of the disk as a function of position along the disk equator. These figures show that the longitude of the ascending node is on the east side of disk. Consequently, only the Hillen et al. (2015) solution with ($i_{\rm d}$, $\Omega_{\rm d}$) = (50°, 125°) satisfies the velocity constraint. If we adopt (50°, 125°), we find $i_{\rm bd} = 96.^\circ5$ and $\Omega_{\rm bd} = 84.^\circ1$. The disk then is $i_{\rm polar} = 8.^\circ7$ away from polar alignment (polar alignment for a massless disk is $i_{\rm bd} = \Omega_{\rm bd} = 90°$). Therefore, the disk is in near polar alignment.

The binary parameters have relatively small uncertainties; however, the disk orientation has larger uncertainties. Therefore, we now consider the range of possible values for $i_{\rm d}$ and $\Omega_{\rm d}$. Figure 2 shows the inclination of the disk away from polar, $i_{\rm polar}$, for the ranges of possible values for the disk angles. A completely polar aligned disk would have $i_{\rm d} = 58°$ and $\Omega_{\rm d} = 121°$, and this is within the uncertainties of the Hillen et al. (2015) measurements.

3. First Polar Planet?

The cavity size of a circumbinary gas disk depends upon the binary separation, the binary eccentricity, and the inclination of the disk relative to the binary orbit. For a disk that is coplanar to the binary orbit, the disk is truncated in the range 2–3 $a_{\rm b}$ depending upon the binary eccentricity (Artymowicz & Lubow 1994). However, this decreases with the inclination of the disk relative to the binary angular momentum vector (Lubow et al. 2015; Miranda & Lai 2015; Lubow & Martin 2018). The size of the binary cavity is therefore an important diagnostic for the inclination of the disk relative to the binary orbit (Franchini et al. 2019). A polar disk may extend down to about 1.6 $a_{\rm b}$.

The polar configuration of the disk in AC Her does not help to explain the large dust cavity since a polar aligned disk has a smaller cavity size than a coplanar disk. The best explanation remains the presence of a planet in the disk. Therefore, this is the first evidence of a polar circumbinary planet! Polar circumbinary planets may form as efficiently as coplanar planets (e.g., Childs & Martin 2021). A planet in a post-AGB star circumbinary disk could be a second-generation planet, meaning a planet that was formed from the material of the post-main-sequence stellar evolution (e.g., Beuermann et al. 2010; Perets 2010; Qian et al. 2011; Zorotovic & Schreiber 2013; Bear & Soker 2014). The observational detection limit of 9 $L_\odot$ in Anugu et al. (2023) is inadequate for detecting this low-contrast tertiary. The tertiary's mass is likely low, considering that its gravitational influence remains unobservable in the binary system's orbit. However, we do not attempt to determine the dynamical limit on the tertiary mass in this paper.

In order for dust filtration to occur, the tertiary must open a gap in the disk (e.g., Zhu et al. 2012). This requires the planet to be sufficiently massive and in an orbit that is coplanar to the disk, otherwise material can spread across the orbital radius of the planet (e.g., Franchini et al. 2020). While there is no observed dust inside of the orbit of the planet, gas may still flow inwards past the planet orbit through gas streams (Artymowicz & Lubow 1996; Lubow & D'Angelo 2006). Therefore we expect there to be a gas disk interior to the planet orbit unless there are multiple planets interior to the putative planet.

If the inner circumbinary disk is fed by material flowing inwards from the outer circumbinary disk, then the inner disk must be coplanar to the outer disk, and therefore also polar to the binary orbit. Further, the timescale for the disk to align to polar is much shorter for the inner disk that is closer to the binary. Since the outer disk is observed to be polar, the inner disk is likely also polar. Warping of the inner disk may be possible if material is added to the disk at an inclination that is misaligned. Disk warping generally occurs in a circumbinary disk that is inclined to the binary orbit. However, a massless polar disk has no warp.

The inner gas disk is predicted to be there observationally since the post-AGB star is depleted in refractory elements suggesting that is is accreting material from the circumbinary disk. The accretion of material onto the companion must also be responsible for the formation of the observed jet (Bujarrabal et al. 2018; Bollen et al. 2020). We discuss this more in Section 4.3.

Figure 1 shows two visualizations of the system. The disk is composed of two rings that are separated by the gap that the putative planet has carved. The outer disk that is observed is composed of gas and dust, while the inner disk that is not observed is composed only of gas.

4. Implications of a Polar Aligned Disk

We consider here a model in which the disk polar alignment in AC Her results from the evolution of an initially moderately misaligned disk to the polar orientation by means of the tidal evolution of a viscous disk (Aly et al. 2015; Martin & Lubow 2017; Lubow & Martin 2018; Zanazzi & Lai 2018; Cuello & Giuppone 2019; Smallwood et al. 2020; Rabago et al. 2023). The application of this model imposes constraints of the origin and evolution of the circumbinary disk.

4.1. Formation of the Circumbinary Disk

Since all observed post-AGB stars with disks are in binaries, the binary must be an essential component to the disk formation. A circumbinary disk that forms misaligned to the binary orbit evolves toward either coplanar alignment or polar alignment depending upon its initial inclination (Martin & Lubow 2017). For a massless disk, the minimum critical inclination relative to the binary orbit is

$$i_{\rm crit} = \sin^{-1}\sqrt{\frac{1-e_{\rm b}^2}{1+4e_{\rm b}^2}} \tag{7}$$

(e.g., Doolin & Blundell 2011), where $e_{\rm b}$ is the binary eccentricity. For $e_{\rm b}=0.2$, we have $i_{\rm crit}=65^\circ$. Therefore the disk must be fed material that has, on average, an inclination greater than this if it is to align to polar. If it is fed material with a lower inclination, then it will align toward coplanar. If the binary orbit had a larger eccentricity in the past, then the critical inclination required for a polar disk would have been lower.

We take the disk age to be of order the post-AGB duration of about $\sim 10^5$ yr (e.g., Izzard & Jermyn 2023). With a precession period of about $\sim 10^4$ yr, a moderately viscous disk can align to polar within its lifetime (e.g., Martin & Lubow 2017).

The nodal precession period for a test particle at orbital radius R that is in a librating orbit is given by

$$t_{\rm prec} = \frac{2\pi}{\omega_{\rm p}} \tag{8}$$

where

$$\omega_{\rm p} = \frac{3\sqrt{5}}{4} e_{\rm b}\sqrt{1+4e_{\rm b}^2}\,\frac{M_1 M_2}{M_{\rm b}^2}\left(\frac{a_{\rm b}}{R}\right)^{7/2}\Omega_{\rm b} \tag{9}$$

(Lubow & Martin 2018), where the total binary mass is $M_{\rm b}=M_1+M_2$ and the binary angular frequency is $\Omega_{\rm b}=\sqrt{GM_{\rm b}/a_{\rm b}^3}$. This was derived in the secular quadrupole approximation using Equations (2.16)–(2.18) in Farago & Laskar (2010). For the parameters of AC Her this is

$$t_{\rm prec} = 1.33\times 10^4\left(\frac{R}{15\ {\rm au}}\right)^{7/2}\ {\rm yr}. \tag{10}$$

This result suggests that a disk with radius of about 15 au can evolve to a polar state over the post-AGB timescale.

A more detailed calculation of a circumbinary disk in which the surface density varies as $\Sigma \propto 1/R$, with inner radius $3a_{\rm b}$ has a precession period of about $\sim 2\times 10^4$ yr if the disk outer radius is about 35 au. With an inner disk radius of $1.6a_{\rm b}$, the same precession period occurs for a disk with outer radius of about 80 au. Such outer radii are smaller than the observed disk outer radius that extends to 1000 au. Such an extension is possible if the disk viscously expands after achieving polar alignment, as discussed in the next subsection.

4.2. Disk Size and Mass

There is a discrepancy between the viscous timescale and the disk lifetime for AC Her. An accretion disk spreads out through the effects of viscosity (Pringle 1981) that is parameterized with

$$\nu = \alpha\left(\frac{H}{R}\right)^2 R^2\Omega_{\rm K}, \tag{11}$$

where α is the Shakura & Sunyaev (1973) viscosity parameter, H/R is the disk aspect ratio, and $\Omega_{\rm K}=\sqrt{GM_{\rm b}/R^3}$ is the Keplerian angular velocity. The viscous timescale in the disk is

$$t_\nu = \frac{R^2}{\nu}, \tag{12}$$

which may be written as

$$t_\nu = 4.5\times 10^3\left(\frac{\alpha}{0.1}\right)^{-1}\left(\frac{H/R}{0.2}\right)^{-2}\left(\frac{R}{30\ {\rm au}}\right)^{3/2}\ {\rm yr}. \tag{13}$$

The disk aspect ratio for these disks is large (e.g., Kluska et al. 2018; Oomen et al. 2020) and we choose an appropriate α parameter for a fully ionized disk (Martin et al. 2019). Hillen et al. (2015) fixed the outer disk radius to 200 au while

Gallardo Cava et al. (2021) suggested the outer parts of the disk extend to 1000 au. The viscous timescale at this radius may be of the order of a million years. This suggests that the disk lifetime must be of this order. However, this is somewhat longer than the disk lifetime suggested by stellar evolution models of up to about 10^5 yr (Izzard & Jermyn 2023).

Hillen et al. (2015) determined the disk dust mass to be greater than $0.001 M_\odot$. As they point out, such a large dust mass would imply a very large gas disk mass for the conventional gas/dust ratio of 100 and instead suggest that lower ratios are more plausible. The angular momentum of a disk with total mass $0.1\,M_\odot$ would likely not allow for a stable polar disk and instead von Zeipel–Kozai–Lidov (ZKL; von Zeipel 1910; Kozai 1962; Lidov 1962) oscillations of the binary would be expected. This has been seen in simulations before in the case of a planet and a star with an outer disk (Terquem & Ajmia 2010). Therefore, we suggest that for AC Her, the total disk angular momentum must be small compared with the binary angular momentum. Indeed, Gallardo Cava et al. (2021) find a total disk mass of $8.1 \times 10^{-4}\,M_\odot$, which would allow for a stable polar aligned disk.

4.3. Feeding of Circumstellar Disks

Simulations show that material in a circumbinary disk can flow inwards through the binary cavity and feed the circumstellar disks around each binary component (e.g., Artymowicz & Lubow 1996; Shi et al. 2012; D'Orazio et al. 2013; Muñoz & Lai 2016; Heath & Nixon 2020; Smallwood et al. 2023). Observationally, accretion of material onto the binary components is inferred in two ways. First, observations show depletion of refractory elements in the atmospheres of some post-AGB stars. All post-AGB stars that are depleted, including AC Her, contain a circumbinary disk. Oomen et al. (2018) suggest that the depletion is due to the accretion of circumbinary disk gas with low dust content onto the star. The low dust content is a consequence of the dust trapping described in the Introduction. Second, a jet is often observed from the main-sequence star. The jet in AC Her is tilted by 6.°5 to the binary angular momentum vector and has a wide opening angle of 30° (Bollen et al. 2022). Jets are thought to be perpendicular to the circumstellar accretion disk that powers them (Blandford & Payne 1982).

The accretion rate from a polar circumbinary disk is similar to that of a coplanar circumbinary disk (Smallwood et al. 2022). A coplanar circumbinary disk feeds the formation of circumstellar disks that are coplanar to the binary orbit. If the circumbinary disk is misaligned to the orbit of the binary, then the circumstellar disks also form misaligned to the binary orbit (e.g., Nixon et al. 2013). In the presence of a polar circumbinary disk, the circumstellar disks that form may also form in a polar orientation (Smallwood et al. 2023).

The circumstellar disk undergoes nodal precession about the binary angular momentum vector (e.g., Papaloizou & Terquem 1995; Larwood et al. 1996; Bate et al. 2000; Lubow & Ogilvie 2000) that, in the presence of dissipation, can lead to coplanar alignment to the binary orbital plane. In addition, for very large misalignments greater than about 40°, the circumstellar disks can undergo ZKL oscillations. The inclination and eccentricity of the circumstellar disk can be exchanged. This can lead on average to a fairly rapid alignment toward the critical ZKL inclination of about 40° (Martin et al. 2014, 2016; Fu et al. 2015; Lubow & Ogilvie 2017; Zanazzi & Lai 2017) but with continuous accretion of high-inclination material it can lead to sustained ZKL oscillations (Smallwood et al. 2021).

For a circumstellar disk with a supply of high-inclination material, there are competing torques from the addition of material that acts to keep the inclination high and from the binary torque that acts toward coplanar alignment (Smallwood et al. 2023). The outcome depends upon the relative strengths of these torques. If the mass accretion dominates, then the disk inclination can remain high. However, if the binary torque dominates then the disk moves toward coplanar alignment by means of tidal dissipation. The disk also undergoes nodal precession when it is misaligned. Therefore the circumstellar disk could be seen at any inclination and longitude of ascending node.

The inclination of a jet that is formed by the circumstellar disk around the companion may be perpendicular to the circumstellar disk. Therefore the orientation of a jet being formed around one component of a binary with a polar circumbinary disk could be in any direction. This is a result of the nodal precession of a misaligned circumstellar disk. This is in contrast to the coplanar circumbinary disk in which the jet orientation would be expected to be close to aligned to the binary angular momentum vector. The large opening angle for the jet in AC Her (Bollen et al. 2022) may be indicative of the nodal precession of a circumstellar disk.

5. Conclusions

We have examined the post-AGB star binary system AC Her and shown that it is within 9° of polar alignment. In a polar alignment, the disk is inclined by 90° to the binary orbital plane with the disk angular momentum vector aligned to the binary eccentricity vector. This is the first observed polar circumbinary disk around a post-AGB star.

The inner edge of the dust disk is much farther out than the tidal truncation radius and a planet within the disk is the most likely explanation. Therefore, this is the first observational evidence of a polar circumbinary planet. While polar gas and debris disks around main-sequence stars have previously been observed, misaligned circumbinary planets have yet to be detected.

The circumbinary disk feeds the formation of circumstellar disks around the binary components. A coplanar circumbinary disk forms coplanar circumstellar disks. However, a polar circumbinary disk forms polar circumstellar disks, but this is not a stable configuration. Polar circumstellar disks may undergo ZKL inclinations oscillations or evolve to coplanarity with the binary. The outcome depends on the competition between the mass accretion torque from the circumbinary disk and the binary torques. Circumstellar disks that are formed from flow from a polar circumbinary disk may be observed at any inclination and orientation.

We describe a model for polar alignment in which the circumbinary disk is initially moderately misaligned with respect to the binary and evolves to polar alignment by means of tidal effects. Material from the post-AGB star that is forming the disk must have an inclination greater than about 65° to the binary orbital plane, assuming the binary eccentricity has not evolved significantly. Smaller initial inclinations are possible if the binary eccentricity had been larger in the past. Such a model requires the disk to have an outer radius of less than 100 au, while the disk has been observed out to ∼1000 au (Bujarrabal et al. 2015). We suggest that this compact disk

expands outwards to reach this larger radius. However, sufficient viscous expansion occurs on timescales of order 10^6 yr that is longer than the duration of the post-AGB phase of about 10^5 yr. More analysis should be carried out to better understand the disk properties.

Acknowledgments

We thank the anonymous referees for useful comments. R.G.M. and S.H.L. acknowledge support from NASA through grants 80NSSC21K0395 and 80NSSC19K0443. This work is based upon observations obtained with the Georgia State University Center for High Angular Resolution Astronomy Array at Mount Wilson Observatory. The CHARA Array is supported by the National Science Foundation under grant Nos. AST-1636624 and AST-2034336. Institutional support has been provided from the GSU College of Arts and Sciences and the GSU Office of the Vice President for Research and Economic Development.

ORCID iDs

Rebecca G. Martin https://orcid.org/0000-0003-2401-7168
Stephen H. Lubow https://orcid.org/0000-0002-4636-7348
David Vallet https://orcid.org/0000-0002-0543-6730
Narsireddy Anugu https://orcid.org/0000-0002-2208-6541
Douglas R. Gies https://orcid.org/0000-0001-8537-3583

References

Aly, H., Dehnen, W., Nixon, C., & King, A. 2015, MNRAS, 449, 65
Anugu, N., Kluska, J., Gardner, T., et al. 2023, ApJ, 950, 149
Artymowicz, P., & Lubow, S. H. 1994, ApJ, 421, 651
Artymowicz, P., & Lubow, S. H. 1996, ApJL, 467, L77
Bate, M. R., Bonnell, I. A., Clarke, C. J., et al. 2000, MNRAS, 317, 773
Bear, E., & Soker, N. 2014, MNRAS, 444, 1698
Beuermann, K., Hessman, F. V., Dreizler, S., et al. 2010, A&A, 521, L60
Blandford, R. D., & Payne, D. G. 1982, MNRAS, 199, 883
Bollen, D., Kamath, D., De Marco, O., Van Winckel, H., & Wardle, M. 2020, A&A, 641, A175
Bollen, D., Kamath, D., Van Winckel, H., et al. 2022, A&A, 666, A40
Bujarrabal, V., Castro-Carrizo, A., Alcolea, J., et al. 2013, A&A, 557, L11
Bujarrabal, V., Castro-Carrizo, A., Alcolea, J., & Van Winckel, H. 2015, A&A, 575, L7
Bujarrabal, V., Castro-Carrizo, A., Van Winckel, H., et al. 2018, A&A, 614, A58
Chen, C., Franchini, A., Lubow, S. H., & Martin, R. G. 2019, MNRAS, 490, 5634
Chen, C., Lubow, S. H., & Martin, R. G. 2020, MNRAS, 494, 4645
Childs, A. C., & Martin, R. G. 2021, ApJL, 920, L8
Corporaal, A., Kluska, J., Van Winckel, H., et al. 2023, A&A, 674, A151
Cuello, N., & Giuppone, C. A. 2019, A&A, 628, A119
Czekala, I., Chiang, E., Andrews, S. M., et al. 2019, ApJ, 883, 22
de Ruyter, S., van Winckel, H., Maas, T., et al. 2006, A&A, 448, 641
Dermine, T., Izzard, R. G., Jorissen, A., & Van Winckel, H. 2013, A&A, 551, A50
Doolin, S., & Blundell, K. M. 2011, MNRAS, 418, 2656
D'Orazio, D. J., & Duffell, P. C. 2021, ApJL, 914, L21
D'Orazio, D. J., Haiman, Z., & MacFadyen, A. 2013, MNRAS, 436, 2997
Doyle, L. R., Carter, J. A., Fabrycky, D. C., et al. 2011, Sci, 333, 1602
Farago, F., & Laskar, J. 2010, MNRAS, 401, 1189
Franchini, A., Lubow, S. H., & Martin, R. G. 2019, ApJL, 880, L18
Franchini, A., Martin, R. G., & Lubow, S. H. 2020, MNRAS, 491, 5351
Francis, L., & van der Marel, N. 2020, ApJ, 892, 111
Fu, W., Lubow, S. H., & Martin, R. G. 2015, ApJ, 807, 75
Gaia Collaboration, Prusti, T., de Bruijne, J. H. J., et al. 2016, A&A, 595, A1
Gallardo Cava, I., Gómez-Garrido, M., Bujarrabal, V., et al. 2021, A&A, 648, A93
Gielen, C., van Winckel, H., Waters, L. B. F. M., Min, M., & Dominik, C. 2007, A&A, 475, 629
Heath, R. M., & Nixon, C. J. 2020, A&A, 641, A64
Hillen, M., de Vries, B. L., Menu, J., et al. 2015, A&A, 578, A40
Hirsh, K., Price, D. J., Gonzalez, J.-F., Ubeira-Gabellini, M. G., & Ragusa, E. 2020, MNRAS, 498, 2936
Izzard, R., & Jermyn, A. 2018, Galax, 6, 97
Izzard, R. G., & Jermyn, A. S. 2023, MNRAS, 521, 35
Kashi, A., & Soker, N. 2011, MNRAS, 417, 1466
Kennedy, G. M., Matrà, L., Facchini, S., et al. 2019, NatAs, 3, 230
Kennedy, G. M., Wyatt, M. C., Sibthorpe, B., et al. 2012, MNRAS, 421, 2264
Kenworthy, M. A., González Picos, D., Elizondo, E., et al. 2022, A&A, 666, A61
Kluska, J., Hillen, M., Van Winckel, H., et al. 2018, A&A, 616, A153
Kluska, J., Van Winckel, H., Coppée, Q., et al. 2022, A&A, 658, A36
Kluska, J., Van Winckel, H., Hillen, M., et al. 2019, A&A, 631, A108
Kozai, Y. 1962, AJ, 67, 591
Larwood, J. D., Nelson, R. P., Papaloizou, J. C. B., & Terquem, C. 1996, MNRAS, 282, 597
Lidov, M. L. 1962, P&SS, 9, 719
Lubow, S. H., & D'Angelo, G. 2006, ApJ, 641, 526
Lubow, S. H., & Martin, R. G. 2018, MNRAS, 473, 3733
Lubow, S. H., Martin, R. G., & Nixon, C. 2015, ApJ, 800, 96
Lubow, S. H., & Ogilvie, G. I. 2000, ApJ, 538, 326
Lubow, S. H., & Ogilvie, G. I. 2017, MNRAS, 469, 4292
Martin, D. V. 2017, MNRAS, 465, 3235
Martin, D. V., & Triaud, A. H. M. J. 2015, MNRAS, 449, 781
Martin, R. G., & Lubow, S. H. 2017, ApJL, 835, L28
Martin, R. G., Lubow, S. H., Nixon, C., & Armitage, P. J. 2016, MNRAS, 458, 4345
Martin, R. G., Nixon, C., Armitage, P. J., Lubow, S. H., & Price, D. J. 2014, ApJL, 790, L34
Martin, R. G., Nixon, C. J., Pringle, J. E., & Livio, M. 2019, NewA, 70, 7
Miranda, R., & Lai, D. 2015, MNRAS, 452, 2396
Muñoz, D. J., & Lai, D. 2016, ApJ, 827, 43
Nixon, C., King, A., & Price, D. 2013, MNRAS, 434, 1946
Oomen, G.-M., Pols, O., Van Winckel, H., & Nelemans, G. 2020, A&A, 642, A234
Oomen, G.-M., Van Winckel, H., Pols, O., et al. 2018, A&A, 620, A85
Orosz, J. A., Welsh, W. F., Carter, J. A., et al. 2012, ApJ, 758, 87
Papaloizou, J. C. B., & Terquem, C. 1995, MNRAS, 274, 987
Perets, H. B. 2010, arXiv:1001.0581
Pinilla, P., Benisty, M., & Birnstiel, T. 2012, A&A, 545, A81
Pinilla, P., Klarmann, L., Birnstiel, T., et al. 2016, A&A, 585, A35
Pringle, J. E. 1981, ARA&A, 19, 137
Qian, S. B., Liu, L., Liao, W. P., et al. 2011, MNRAS, 414, L16
Rabago, I., Zhu, Z., Martin, R. G., & Lubow, S. H. 2023, MNRAS, 520, 2138
Sahai, R., Claussen, M. J., Schnee, S., Morris, M. R., & Sánchez Contreras, C. 2011, ApJL, 739, L3
Sepinsky, J. F., Willems, B., & Kalogera, V. 2007a, ApJ, 660, 1624
Sepinsky, J. F., Willems, B., Kalogera, V., & Rasio, F. A. 2007b, ApJ, 667, 1170
Shakura, N. I., & Sunyaev, R. A. 1973, A&A, 24, 337
Shi, J.-M., Krolik, J. H., Lubow, S. H., & Hawley, J. F. 2012, ApJ, 749, 118
Smallwood, J. L., Franchini, A., Chen, C., et al. 2020, MNRAS, 494, 487
Smallwood, J. L., Lubow, S. H., & Martin, R. G. 2022, MNRAS, 514, 1249
Smallwood, J. L., Martin, R. G., & Lubow, S. H. 2021, ApJL, 907, L14
Smallwood, J. L., Martin, R. G., & Lubow, S. H. 2023, MNRAS, 520, 2952
Terquem, C., & Ajmia, A. 2010, MNRAS, 404, 409
Van Winckel, H., Waelkens, C., Waters, L. B. F. M., et al. 1998, A&A, 336, L17
von Zeipel, H. 1910, AN, 183, 345
Welsh, W. F., Orosz, J. A., Carter, J. A., et al. 2012, Natur, 481, 475
Zanazzi, J. J., & Lai, D. 2017, MNRAS, 467, 1957
Zanazzi, J. J., & Lai, D. 2018, MNRAS, 473, 603
Zhu, Z., Nelson, R. P., Dong, R., Espaillat, C., & Hartmann, L. 2012, ApJ, 755, 6
Zhu, Z., Stone, J. M., & Rafikov, R. R. 2013, ApJ, 768, 143
Zorotovic, M., & Schreiber, M. R. 2013, A&A, 549, A95
Zrake, J., Tiede, C., MacFadyen, A., & Haiman, Z. 2021, ApJL, 909, L13